HHS Public Access

Author manuscript

J Alzheimers Dis. Author manuscript; available in PMC 2018 May 04.

Published in final edited form as:

J Alzheimers Dis. 2018 ; 61(1): 401–414. doi:10.3233/JAD-170557.

SPARCL1 Accelerates Symptom Onset in Alzheimer's Disease and Influences Brain Structure and Function During Aging

Sahba Seddighi[a], **Vijay R. Varma**[a], **Yang An**[b], **Sudhir Varma**[c], **Lori L. Beason-Held**[b], **Toshiko Tanaka**[d], **Melissa H. Kitner-Triolo**[b], **Michael A. Kraut**[e], **Christos Davatzikos**[f], and **Madhav Thambisetty**[a,*]

[a]Clinical and Translational Neuroscience Unit, Laboratory of Behavioral Neuroscience, National Institute on Aging (NIA), National Institutes of Health (NIH), Baltimore, MD, USA

[b]Laboratory of Behavioral Neuroscience, National Institute on Aging, Baltimore, MD, USA

[c]HiThru Analytics, Laurel, MD, USA

[d]Translational Gerontology Branch, National Institute on Aging, Baltimore, MD, USA

[e]Department of Radiology and Radiological Sciences, Johns Hopkins University School of Medicine, Baltimore, MD, USA

[f]Department of Radiology, Center for Biomedical Image Computing and Analytics, University of Pennsylvania, Philadelphia, PA, USA

Abstract

We recently reported that alpha-2 macroglobulin (A2M) is a biomarker of neuronal injury in Alzheimer's disease (AD) and identified a network of nine genes co-expressed with A2M in the brain. This network includes the gene encoding SPARCL1, a protein implicated in synaptic maintenance. Here, we examine whether *SPARCL1* is associated with longitudinal changes in brain structure and function in older individuals at risk for AD in the Baltimore Longitudinal Study of Aging. Using data from the Gene-Tissue Expression Project, we first identified two single nucleotide polymorphisms (SNPs), rs9998212 and rs7695558, associated with lower brain *SPARCL1* gene expression. We then analyzed longitudinal trajectories of cognitive performance in 591 participants who remained cognitively normal (average follow-up interval: 11.8 years) and 129 subjects who eventually developed MCI or AD (average follow-up interval: 9.4 years). Cognitively normal minor allele carriers of rs7695558 who developed incident AD showed accelerated memory loss prior to disease onset. Next, we compared longitudinal changes in brain volumes (MRI; n = 120 participants; follow-up = 6.4 years; 826 scans) and resting-state cerebral blood flow (rCBF; ^{15}O-water PET; n = 81 participants; follow-up = 7.7 years; 664 scans) in cognitively normal participants. Cognitively normal minor allele carriers of rs9998212 showed

*Correspondence to: Madhav Thambisetty, Chief, Unit of Clinical and Translational Neuroscience, Laboratory of Behavioral Neuroscience, National Institute on Aging, 251 Bayview Blvd, Baltimore, MD 21224, USA. Tel.: +1 410 558 8572; Fax: +1 410 558 8674; thambisettym@mail.nih.gov.

Handling Associate Editor: Ravi Rajmohan

Authors' disclosures available online (http://j-alz.com/manuscript-disclosures/17-0557r1).

SUPPLEMENTARY MATERIAL

The supplementary material is available in the electronic version of this article: http://dx.doi.org/10.3233/JAD-170557.

accelerated atrophy in several global, lobar, and regional brain volumes. Minor allele carriers of both SNPs showed longitudinal changes in rCBF in several brain regions, including those vulnerable to AD pathology. Our findings suggest that *SPARCL1* accelerates AD pathogenesis and thus link neuroinflammation with widespread changes in brain structure and function during aging.

Keywords

Alzheimer's disease; magnetic resonance imaging; positron emission tomography; single nucleotide polymorphism

INTRODUCTION

In the United States alone, Alzheimer's disease (AD) currently affects over 5.4 million individuals and, if left unchecked, is projected to impose an unparalleled economic and healthcare burden by 2050—nearly tripling in prevalence and driving healthcare costs to an estimated $1 trillion [1]. The development of effective preventive strategies and disease-modifying therapies depends on understanding the molecular mechanisms that underpin AD. The predominant strategy for disease modification in AD has been to enhance the clearance or inhibit the deposition of amyloid-β (Aβ) in the brain. However, the repeated failures of pivotal phase-III clinical trials of anti-Aβ treatments have highlighted the importance of understanding other molecular pathways that may be plausible targets for disease modification [2–4]. Previous epidemiological studies have suggested that systemic inflammation is an important risk factor for AD, while emerging evidence indicates that modulating the inflammatory/immune response during the early stages of AD pathogenesis may be a promising approach to disease modification [5, 6].

In a recent study exploring the role of systemic inflammation in preclinical AD, we reported that serum concentration of alpha-2 macroglobulin (A2M), a major component of the innate immune system, is associated with risk of incident AD, reflects early neuronal injury, and may be responsive to tau phosphorylation states in the brain. We also identified a network of nine co-regulated genes that jointly contribute to predicting the gene expression of *A2M* [7]. Within this network of *A2M*-associated genes that may modulate responses to neuronal injury in AD, *SPARCL1* (Secreted Protein Acidic and Rich in Cysteine-Like 1) is of particular interest in view of its potential roles in synaptic function. The SPARCL1 protein has been previously studied in the context of neuronal development for its synaptogenic properties [8]. However, recent evidence suggests that the expression of this protein continues into adulthood, is markedly upregulated during central nervous system (CNS) injury or disease, and is likely to aid in the reconstruction of neuronal circuits [9–11]. Interestingly, a number of psychiatric and neurological disorders, including depression, schizophrenia, autism, and multiple sclerosis, have thus far been linked to dysregulation in SPARCL1 expression—suggesting that SPARCL1 may be critical in maintaining healthy CNS function [12–18]. Together with previous reports of altered levels of SPARCL1 in the cerebrospinal fluid (CSF) of AD patients, it is plausible that perturbations in SPARCL1 regulation are important in the pathogenesis of AD [19–21].

Synaptic loss is an early feature of AD that renders neurons dysfunctional and prone to irreversible death, ultimately precipitating the severe brain atrophy and cognitive impairment observed in later stages of the disease [22]. As SPARCL1 closely regulates the formation, maintenance, and repair of synapses [23], we sought to investigate associations between polymorphic variation in the *SPARCL1* gene and brain structure and function in preclinical AD. In this study, we examined associations between single nucleotide polymorphisms (SNPs) in the *SPARCL1* gene and longitudinal changes in cognitive performance, brain volumes, and regional resting-state cerebral blood flow (rCBF) in older individuals in the Baltimore Longitudinal Study of Aging (BLSA).

MATERIALS AND METHODS

An overview of the study design, including datasets used in the current analyses, is provided in Fig. 1.

Identification of SPARCL1 gene: Gene Expression Omnibus (GEO) Repository

We identified *SPARCL1* as a member of an '*A2M* network' of co-expressed genes using the ExplainBio web tool, as previously reported [7, 24, 25] (Supplementary Figures 1 and 2). Using a selection of publicly available microarray data on normal subjects from the National Center for Biotechnology Information (NCBI) Gene Expression Omnibus (GEO) repository, the tool applies an iterative algorithm to generate a network in which the expression of a target gene is modeled as a linear combination of one or more source genes. All GEO data are collected under compliance with the NIH Genomic Data Sharing Policy, which provides protection for publicly available human genomic data. Additional information regarding Explainbio has been previously described in detail [7].

Selection of SPARCL1 SNPs: Genotype-Tissue Expression (GTEx) Project

We downloaded expression quantitative trait loci (eQTL) results for all tissues from the Genotype-Tissue Expression (GTEx) Project portal [26] (Supplementary Figure 1). We queried SNPs that were significantly associated with *SPARCL1* gene expression (False Discovery Rate (FDR) Q value <0.05) in the brain. Regional gene expression data were collected from twelve brain regions in the GTEx Project (Supplementary Material). *P*-values and normalized beta coefficients were generated using methodology defined by the GTEx consortium [26]. *P*-values were adjusted for multiple comparisons by computing the Q-value [1], and a Q-value cutoff of 0.05 was imposed to detect significantly associated SNPs [27].

We extracted and excluded SNPs in high linkage disequilibrium (1000 Genomes Pilot 1 dataset, CEU population panel, distance limit 500) within each of the brain regions associated with *SPARCL1* eQTLs [28] (Supplementary Figure 3). For SNPs in high linkage disequilibrium ($r^2 > 0.6$), the variant with the highest beta coefficient was selected.

Genotyping of SPARCL1 SNPs: Baltimore Longitudinal Study of Aging (BLSA)

Genome-wide genotyping was performed using the Illumina Infinium HumanHap550 genotyping chip, which assays over 555,000 unique SNPs per sample. Standard quality control of genotyping data was conducted as described previously [29]. Briefly, individuals

were excluded due to call rate < 95% genome-wide, cryptic relatedness due to proportional sharing (pi_hat) > 0.125 with another participant in the BLSA (effectively excluding first degree relatives), and non-European ancestry ascertained from multi-dimensional scaling analyses using HapMap reference populations. SNPs were excluded due to minor allele frequencies (MAF) < 1%, a missingness rate > 5%, Hardy-Weinberg equilibrium *p*-values < 1E-5, and non-random missingness by haplotype *p*-values < 1E-5. All quality control of genotype data was undertaken using PLINKv1.05 [PMID: 17701901]. Using 544892 SNPs that passed QC, imputation of 1000 genome SNPs was conducted using Minimac with integrated 1000G Phase I Integrated Release Version 3 Haplotypes as reference (PMID: 22820512).

Participants and methods: BLSA

BLSA is a prospective cohort study of aging in community-dwelling individuals that began in 1958. The volunteer participants are predominantly white individuals with an above-average education level. A general description of the study population, enrollment procedures, and criteria has been reported previously [30]. Briefly, the BLSA continuously enrolls healthy volunteers aged 20 and older who are followed for life, regardless of changes in health and functional status. Presently, participants are examined over three days of testing at the NIA Clinical Research Unit in Baltimore at intervals of one to four years, with more frequent follow-up visits for older participants. Certified nurse practitioners and technicians administer all assessments according to standardized protocols [30, 31]. Diagnoses of mild cognitive impairment (MCI) (Petersen criteria [32]), dementia, and AD (DSM-III-R and NINCDS-ADRA criteria, respectively [33, 34]) are made at consensus case conferences.

Clinical and neuropsychological data were reviewed at consensus case conferences if participants made four or more errors on the Blessed Information Memory Concentration (BIMC) test [35], if their Clinical Dementia Rating (CDR) score was equal to or greater than 0.5, or if concerns were raised about their cognitive status. The CDR was used in the BLSA as an estimate of everyday functioning based on a previous level of functioning to determine if participants exhibited symptoms of MCI. The CDR is a semi-structured interview where both the participant and an informant who knows the participant well are asked questions with respect to six different cognitive domains (i.e., memory, orientation, language and problem solving, home and hobbies, community affairs, and personal care) [36]. The total CDR score is based on the scores from all six domains, from both participants and their informants, where scores of 0 indicate normal everyday functioning and scores of 0.5 are consistent with MCI. The CDR was combined with serial psychometric testing, medical history, physical examination, blood work, and neuroimaging during a consensus case conference to adjudicate identified participants as exhibiting normal cognitive function or MCI. All participants were also screened for depression with the Center for Epidemiologic Studies Depression Scale (CESD) [37].

The study was approved by the Institutional Review Board and the National Institute on Aging. Human research at the National Institutes of Health (NIH) is implemented in accord with the U.S. Department of Health and Human Services (45 CFR46) and U.S. Food and

Drug Administration (21 CFR 50 and 56) regulations for the protection of human subjects. The NIA IRB is part of the Human Subject Protection Program of the NIH. All participants provided written informed consent at each visit [38, 39].

To examine associations between *SPARCL1* variants and longitudinal changes in brain structure and function, we analyzed two complementary datasets from the BLSA (Fig. 1 & Supplementary Figure 1).

The first dataset analyzed was the main BLSA study, where the principal objective was to examine the effect of *SPARCL1* SNPs on rates of cognitive decline, both in cognitively normal individuals (i.e., non-converters; NC) and in those who developed incident MCI/AD (i.e., converters) during follow up. In this analysis, we grouped cognitively normal individuals progressing to incident MCI together with those converting to incident AD with the rationale that MCI individuals represent prodromal AD. Moreover, this allowed us to adequately power these analyses as the relatively small sample size precluded stratification by MCI and AD separately. As our main goal was to test associations between *SPARCL1* SNPs and longitudinal changes in cognitive performance during the preclinical stages of AD pathogenesis (i.e., prior to symptom onset), all cognitive data in the converter group after the onset of cognitive impairment were excluded. Longitudinal data were available for 591 participants in the NC group (mean age at first assessment: 61.3 years; range: 45–93 years; total number of assessments: 3,672; rs7695558 : 163, rs9998212 : 169), who were followed for an average of 11.8 years. In the converters group, 129 participants, who were initially cognitively normal (mean age at first assessment: 73 years; range: 60–89 years; total number of assessments: 838; rs7695558 : 32, rs9998212 : 37), converted to either incident amnestic MCI ($n = 39$) or AD ($n = 90$) during the follow-up interval of 9.4 years. Further details of sample characteristics for the analyses of trajectories of cognitive performance (risk allele carriers versus non-carriers) are provided in Table 1A and B.

The second dataset analyzed was from the neuroimaging substudy of the BLSA (BLSA-NI), which began in 1994. BLSA participants were initially prioritized for admission to the neuroimaging study based on health considerations and the amount of previous cognitive data available for each individual. At enrollment, participants were free of self-reported central nervous system disease, severe cardiac disease, pulmonary disease, or metastatic cancer and underwent annual or semi-annual imaging and clinical evaluations. The neuroimaging substudy of the BLSA has been described in detail previously [40, 41]. We analyzed both MRI ($n = 120$ participants; mean age at first assessment: 70.4; range: 56–85 years old; rs7695558 : 30, rs9998212 : 35) and ^{15}O-water positron emission tomography (PET) ($n = 81$ participants; mean age at first assessment: 69.5; range: 56–85 years old; rs7695558 : 21, rs9998212 : 24) scans from individuals who also had genome-wide genotyping data available. Of those whose MRI scans were analyzed, 13 were diagnosed with MCI during the course of the study, 4 were diagnosed with dementia, and 1 was diagnosed with non-MCI cognitive impairment. Only data prior to the onset of cognitive impairment were included in the MRI analyses. Of individuals whose MRI scans were analyzed, 81 had at least three ^{15}O-water PET scan visits; these participants remained cognitively normal throughout the neuroimaging interval. Further details of sample characteristics for BLSA-NI substudy are provided in Table 2.

Neuropsychological testing

During each BLSA visit, participants completed a battery of neuropsychological tests. We evaluated the association of *SPARCL1* with the following five domains of cognitive performance: memory, attention, executive function, language, and visuospatial ability. We used standardized scores of each cognitive measure, based on the means and standard deviations at the baseline assessments, to compute composite measures for the cognitive domains. Memory was the mean of the immediate free recall summary score (five trials) and delayed free recall on the California Verbal Learning Test (CVLT). Language was the mean of the Letter (i.e., FAS) and Category Fluency Tests. Attention was the mean of Trail-Making A and the Digit Span Forward subtest of the Wechsler Adult Intelligence Scale-Revised. Executive function was the mean of Trail-Making B and Digits Backward. Visuospatial ability was defined by the mean of the Card Rotations Test and Clock-to-Command drawing score.

SPARCL1 and longitudinal changes in brain volumes

MRI acquisition and processing—MRI scans were acquired using a GE Signa 1.5T scanner (Milwaukee, WI) with high-resolution spoiled-GRASS (gradient recalled acquisition in the steady state) axial series (repetition time = 35 ms, echo time = 5 ms, field of view = 24 cm, flip angle = 45°, matrix = 256 × 256). All scanning and image processing methods have been previously described [42–44]. Data from MRI scans obtained annually from baseline to the last available follow-up were used in the analyses. MRI data after the onset of cognitive impairment in converters to MCI/AD were excluded. The mean interval between baseline and last follow-up MRI scan was 6.4 (±2.7 SD) years.

Briefly, images were corrected for rotation and head tilt and reformatted parallel to the anterior–posterior commissure plane. Extracranial tissue was removed using a semi-automated procedure in combination with manual editing. Images were then segmented into CSF, white matter (WM), and gray matter (GM). Finally, scans were realigned and spatially normalized into standard stereotactic space and data from regions of interest were quantified. A template-based deformation approach was applied using the ICBM standard MRI (Montreal Neurologic Institute) as the template and a hierarchical elastic matching algorithm for deformation and regions of interest determination [43]. All images were normalized individually to the same template. The RAVENS approach (regional analysis of volumes examined in normalized space) [42] was used, in which local values of tissue density maps (one for GM, one for WM, and one for CSF) reflect the amount of respective tissue in the vicinity of a voxel. Tissue densities are mathematical quantities measuring local tissue volumes and do not reflect any microstructural physical density of brain tissue. The template warping algorithm, modified for head image registration, was used to determine intracranial volume (ICV) [45].

Regional GM and WM volumes throughout the entire brain were examined in this study, including frontal gyrus (superior, middle, inferior, medial, orbito-frontal), sensorimotor cortex (precentral, post-central), parietal gyrus (superior, supramarginal, angular), temporal lobe (superior, middle, inferior, parahippocampal gyrus, entorhinal cortex, perirhinal cortex,

hippocampus), occipital gyrus (superior, middle, inferior, and occipito-temporal), cingulate gyrus, insula, precuneus, and cuneus.

SPARCL1 and longitudinal changes in rCBF

^{15}O-Water PET acquisition and processing—PET measures of rCBF were obtained using [^{15}O] water as previously described [46]. For each scan, 75 mCi of [^{15}O] water was injected as a bolus. Scans were performed on a GE 4096+ scanner, which provides 15 slices of 6.5 mm thickness. Images were acquired for 60 s from the time total radioactivity counts in the brain reached threshold level. Attenuation correction was performed using a transmission scan acquired prior to the emission scans. Each imaging session included a resting scan in which participants were instructed to keep their eyes open and focused on a computer screen covered by a black cloth.

Data from PET scans obtained annually from baseline to the last available follow-up time points were used in the analyses. The mean interval between baseline and last follow-up PET scan was 7.7 (±1 SD) years. PET scans were realigned and spatially normalized into standard stereotactic space and smoothed to full width at half maximum of 12 × 12 × 12 mm in the x, y, and z planes using a Gaussian filter. To control for variability in global flow, rCBF values at each voxel were ratio adjusted to the mean global flow estimated from gray matter intensity values and scaled to 50 ml/100 g/min for each scan.

For each participant, change in rCBF was calculated across all preprocessed scans using linear modeling to estimate the rates of change over time and extract the estimated fit parameter for each voxel. An image of the longitudinal rates of change at each voxel (i.e. slope or linear temporal trends image) was then created for each participant (Statistical Parametric Mapping software, SPM2, Wellcome Trust Centre for Neuroimaging, UCL, London).

Statistical analyses

The analyses reported herein are based on data collected within the BLSA (including the neuroimaging substudy; BLSA-NI), an ongoing observational study. As indicated in Fig. 1, we used all available data from BLSA and BLSA-NI participants who had both genotyping data (to determine *SPARCL1* SNP status), as well as longitudinal measures of cognitive performance, brain volumes (from MRI scans), and resting-state cerebral blood flow (rCBF from ^{15}O-water PET).

SPARCL1 and longitudinal changes in cognitive performance

Linear mixed effects models [46] were used to investigate associations between rs7695558 and rs9998212 SNP variants in the *SPARCL1* gene and longitudinal trajectories of domain-specific cognitive performance in the converter and NC groups separately.

The fixed effects part of the model included the following predictors: *SPARCL1* SNP minor allele carrier status, baseline age, baseline age squared, sex, years of education, follow-up interval, and interactions of interval with SNP, baseline age, and sex. Random effects included intercept and interval with unstructured covariance. This model allowed us to

investigate associations between *SPARCL1* risk allele(s) and baseline cognitive performance as well as longitudinal changes in cognitive performance after adjusting for baseline age, education, and sex. The NC and MCI/AD samples were independently analyzed.

Effect size was calculated using the difference between mean rates of change in domain-specific cognitive performance in carriers and non-carriers of the minor allele, divided by the standard deviation of rates of change in domain-specific cognitive performance.

SPARCL1 and longitudinal changes in brain volumes

Separate linear mixed effects models were also used for longitudinal analyses of associations between *SPARCL1* SNPs and rates of change in brain volumes [43, 47], with each regional brain volume used as an outcome variable. The fixed effects included intracranial volume, SNP, sex, baseline age, interval and interactions of interval with SNP, sex, and baseline age. Random effects included intercept and interval with unstructured covariance. Due to the limited number of participants who developed MCI/AD in the BLSA-NI study, we did not separately model converters and non-converters for MRI and PET (below) analyses.

The models were fit using PROC MIXED procedure in SAS 9.4 (SAS Institute, Cary, NC) software.

Effect size was calculated using the difference between mean rates of change in brain volumes in carriers and non-carriers of the minor allele, divided by the standard deviation of rates of change in brain volumes.

SPARCL1 and longitudinal changes in rCBF

Slope images were used from all participants in a voxel-based multiple regression analysis (SPM5), where the rs7695558 and rs9998212 SNPs were used as independent predictors of longitudinal changes in rCBF. The associations were adjusted for baseline age, sex, and the interval between baseline and last scans. In order to reduce the risk of Type-I error due to multiple comparisons, we adopted two procedures in the analyses of the rCBF PET data. We first applied a statistical magnitude threshold of $p < 0.005$, as recommended by the PET Working Group of the NIH/NIA Neuroimaging Initiative. Secondly, we applied a spatial extent threshold of at least 50 voxels within the regions meeting the statistical threshold of $p < 0.005$, as reported previously [48].

RESULTS

Selection of SPARCL1 SNPs

Supplementary Figure 2 shows the network of genes, including *SPARCL1*, that are co-expressed with *A2M*, encoding A2M, an acute phase protein that we recently reported is associated with neuronal injury in early stages of AD pathogenesis [7].

Using expression quantitative trait loci (eQTL) data from the Gene Tissue Expression (GTEx) Project, we identified eleven *SPARCL1* SNPs that were significantly associated with *SPARCL1* expression in the brain (Supplementary Figure 3). All identified SNPs had negative beta values, indicating that carrying the minor allele is associated with decreased

SPARCL1 gene expression in the brain. Information on SNP rs60614311 was unavailable in the Broad Institute Proxy Search; this variant was thus excluded from subsequent analyses. Of the ten remaining SNPs, five were significantly correlated with *SPARCL1* expression in the frontal cortex, and five were significantly correlated with *SPARCL1* expression in the hippocampus (Supplementary Table 1). SNPs associated with *SPARCL1* expression in the cortex were in high linkage disequilibrium ($r^2 > 0.6$), as were SNPs associated with *SPARCL1* expression in the hippocampus (Supplementary Figure 3). From each of these brain regions, the variant with the highest absolute beta coefficient was selected for all further analyses. Subsequent analyses thus focused on rs7695558 and rs9998212, associated with *SPARCL1* expression in the frontal cortex (Broadmann area 9; BA9) and hippocampus, respectively. Both SNPs had a minor allele frequency of 0.15 in the BLSA. This value was consistent among converters and non-converters.

SPARCL1 and longitudinal changes in cognitive performance

In cognitively normal individuals, there were no significant differences in trajectories of cognitive performance between minor allele carriers versus non-carriers of the rs7695558 and rs9998212 SNPs in *SPARCL1*. Among individuals who developed incident MCI/AD (i.e., converters), minor allele carriers of the rs7695558 SNP in *SPARCL1* showed accelerated declines in memory performance during the presymptomatic stages of disease progression ($\beta = -0.606$; $p = 0.0224$) (Fig. 2). The minor allele of the rs9998212 variant was not associated with differential rates of cognitive decline in carriers versus non-carriers. These results remained unchanged in sensitivity analyses after excluding individuals with non-AD MCI ($n = 22$).

SPARCL1 and longitudinal changes in brain volumes

In the MRI study, 37 data points after the onset of incident cognitive impairment were excluded. We also confirmed that the distribution of individuals converting to AD/MCI in the MRI analyses was similar between the minor allele carriers and non-carriers for both SNPs (Fisher's Exact Test $p = 1.00$ and $p = 0.838$ for rs7695558 and rs9998212, respectively). In cognitively normal individuals, carriers of the minor allele of the rs9998212 variant in *SPARCL1* showed accelerated rates of brain atrophy in several global (total gray matter, $\beta = -0.7573$; $p = 0.0078$; total ventricular volume, $\beta = 0.1849$; $p = 0.0029$), lobar (frontal gray matter, $\beta = -0.3412$; $p = 0.0023$; parietal gray matter, $\beta = -0.258$; $p = 0.0006$), and regional brain volumes (inferior frontal gyrus, $\beta = -0.06344$; $p = 0.0494$; medial frontal gyrus, $\beta = -0.08553$; $p = 0.0017$; orbitofrontal gyrus, $\beta = -0.07195$; $p = 0.0023$; post-central sensorimotor cortex, $\beta = -0.1023$; $p = 0.0067$; superior parietal lobule, $\beta = -0.0897$; $p = 0.0111$) relative to non-carriers (Fig. 3). The *SPARCL1* rs7695558 SNP was not associated with differential rates of brain atrophy between minor allele carriers and non-carriers.

SPARCL1 and longitudinal changes in rCBF

Minor allele carriers of both the rs7695558 and rs9998212 SNPs showed significant differences in longitudinal changes in rCBF relative to non-carriers. Compared to non-carriers, minor allele carriers of the rs7695558 SNP showed significantly greater decreases in rCBF within the superior temporal, medial frontal, and orbitofrontal cortices.

Significantly greater longitudinal increases in rCBF were observed in minor allele carriers of rs7695558 within the inferior temporal gyrus, cerebellum, and cuneus, relative to non-carriers.

Compared to non-carriers, minor allele carriers of the rs9998212 SNP showed significantly greater decreases in rCBF within the anterior cingulate and superior temporal gyri, as well as the insula. Significantly greater longitudinal increases in rCBF were observed in minor allele carriers of rs9998212 within the lingual, inferior temporal, and middle occipital gyri, as well as the cerebellum and precuneus (Table 3; Fig. 4).

DISCUSSION

We recently identified *SPARCL1* as a member of a network of genes linked to neuronal injury in preclinical AD. We therefore hypothesized that the *SPARCL1* gene, encoding SPARCL1, a known synaptogenic protein implicated in neuronal repair [49, 50], is associated with AD-related endophenotypes during preclinical stages of the disease. We first confirmed regionally specific gene expression of *SPARCL1* in the brain within the frontal cortex and hippocampus. We then showed that *SPARCL1* variants that correlate with lower brain gene expression levels are associated with accelerated cognitive decline during preclinical AD and faster rates of brain atrophy during aging. Finally, we showed that these *SPARCL1* variants are associated with regionally specific longitudinal changes in neuronal activity in areas related to higher-order cognitive processing, as well as within brain regions vulnerable to AD pathology in older individuals. To the best of our knowledge, this is the first study to implicate the *SPARCL1* gene in AD pathogenesis using longitudinal cognitive and neuroimaging data in older individuals.

Our novel findings complement and extend previous studies in post-mortem human brain tissue samples showing lower gene expression of *SPARCL1* in the hippocampus of AD patients relative to controls, as well proteomic analyses in CSF showing altered levels of SPARCL1 protein in AD [20, 51]. Our results suggest that polymorphic variations in *SPARCL1* that are associated with lower gene expression in the brain accelerate symptom onset in AD through perturbations in neuronal activity and faster rates of brain atrophy in at-risk individuals. In interpreting our ^{15}O-water PET results, we propose that longitudinal decrements in rCBF in brain regions mediating higher-order cognitive processes, such as the superior temporal and medial frontal cortices, represent early signatures of failing synaptic function related to lower *SPARCL1* gene expression [52–54]. Conversely, brain regions showing longitudinal increases in rCBF may represent compensatory changes in neuronal activity that may be recruited to maintain normal cognitive function in at-risk individuals [55–57]. In this context, it is striking that minor allele carriers of *SPARCL1* show greater longitudinal increases in rCBF in the precuneus and inferior temporal cortex, which are brain regions especially vulnerable to Aβ deposition and tau accumulation, respectively [58, 59]. While it is plausible that increasing rCBF observed in these brain regions reflects early compensatory changes or neuroexcitatory responses to accumulating age-related neuropathology in at-risk individuals, the long-term consequences of increasing neuronal activity may include Aβ accumulation and neurodegeneration within vulnerable brain regions [60–63].

Interestingly, recent studies suggest that dysregulation of excitatory glutamatergic neurotransmission by Aβ is associated with synaptic loss, as well as tau phosphorylation [64, 65]. Furthermore, our findings are relevant in the context of a recent report showing that SPARCL1 mediates linkage of the cell adhesion molecules neurexin-1-alpha and neuroligin-1B, a critical step in the formation of glutamatergic synapses [66, 67].

The key strengths of our study are the well characterized BLSA cohort with serial cognitive and neuroimaging assessments over a long follow-up interval, as well as adjudicated diagnoses of incident MCI/AD. Some important limitations include the limited sampling of cortical brain regions in the GTEx study that we used to identify *SPARCL1* eQTLs in the brain. As these data were available in only the frontal and anterior cingulate cortices, we were unable to comprehensively evaluate regional differences in *SPARCL1* gene expression across the brain. This is an important consideration in the interpretation of both our longitudinal cognitive data, as well as imaging measures. Thus, observed effects of the rs9998212 SNP (associated with lower *SPARCL1* gene expression in the hippocampus) on accelerated brain atrophy in several cortical regions may be mediated by similarly reduced gene expression in these regions that we were unable to analyze. Similarly, the observed effects of the rs7695558 SNP (associated with lower *SPARCL1* gene expression in the frontal cortex) on accelerated memory decline may represent net effects of altered gene expression in several other brain regions that we did not test. Subsequent analyses of global *SPARCL1* gene expression levels across several brain regions may allow for greater understanding of the net effects of altered gene expression impacting specific AD-related endophenotypes. Secondly, the relatively small number of converters to MCI/AD in our MRI and ^{15}O-water PET studies precluded stratified analyses in these individuals relative to controls. While our results provide novel evidence linking *SPARCL1* with AD pathogenesis, the precise molecular mechanisms underlying these associations must await additional studies in relevant experimental models. The generalizability of our findings also merits further testing in independent cohorts.

In summary, we have demonstrated that the *SPARCL1* gene accelerates both symptom onset in AD and brain atrophy during aging. These effects may be mediated through lower gene expression of *SPARCL1* in the brain and alterations in synaptic function. Our findings open new lines of investigation into the role of *SPARCL1* in the early stages of AD pathogenesis.

Supplementary Material

Refer to Web version on PubMed Central for supplementary material.

Acknowledgments

We are grateful to the Baltimore Longitudinal Study of Aging participants and neuroimaging staff for their dedication to these studies and the staff of the Johns Hopkins University PET facility for their assistance.

This research was supported by the Intramural Research Program of the NIH, National Institute on Aging, and by Research and Development Contract N01-AG-3-2124.

The Genotype-Tissue Expression (GTEx) Project was supported by the Common Fund of the Office of the Director of the National Institutes of Health. Additional funds were provided by the NCI, NHGRI, NHLBI, NIDA, NIMH, and NINDS. Donors were enrolled at Biospecimen Source Sites funded by NCI\SAIC-Frederick, Inc. (SAIC-F)

subcontracts to the National Disease Research Interchange (10XS170), Roswell Park Cancer Institute (10XS171), and Science Care, Inc. (X10S172). The Laboratory, Data Analysis, and Coordinating Center (LDACC) was funded through a contract (HHSN268201000029C) to The Broad Institute, Inc. Biorepository operations were funded through an SAIC-F subcontract to Van Andel Institute (10ST1035). Additional data repository and project management were provided by SAIC-F (HHSN261200800001E). The Brain Bank was supported by supplements to University of Miami grants DA006227 & DA033684 and to contract N01MH000028. Statistical Methods development grants were made to the University of Geneva (MH090941 & MH101814), the University of Chicago (MH090951, MH090937, MH101820, MH101825), the University of North Carolina – Chapel Hill (MH090936 & MH101819), Harvard University (MH090948), Stanford University (MH101782), Washington University St Louis (MH101810), and the University of Pennsylvania (MH101822). The data used for the analyses described in this manuscript were obtained from the GTEx Portal on 06/10/2015.

References

1. Ryan NS, Rossor MN, Fox NC. Alzheimer's disease in the 100 years since Alzheimer's death. Brain. 2015; 138:3816–3821. [PubMed: 26541346]
2. Skaper SD. Alzheimer's disease and amyloid: Culprit or coincidence? Int Rev Neurobiol. 2012; 102:277–316. [PubMed: 22748834]
3. Iqbal K, Liu F, Gong CX. Alzheimer disease therapeutics: Focus on the disease and not just plaques and tangles. Biochem Pharmacol. 2014; 88:631–639. [PubMed: 24418409]
4. Ising C, Stanley M, Holtzman DM. Current thinking on the mechanistic basis of Alzheimer's and implications for drug development. Clin Pharmacol Ther. 2015; 98:469–471. [PubMed: 26250900]
5. Heneka MT, Carson MJ, El Khoury J, Landreth GE, Brosseron F, Feinstein DL, Jacobs AH, Wyss-Coray T, Vitorica J, Ransohoff RM, Herrup K, Frautschy SA, Finsen B, Brown GC, Verkhratsky A, Yamanaka K, Koistinaho J, Latz E, Halle A, Petzold GC, Town T, Morgan D, Shinohara ML, Perry VH, Holmes C, Bazan NG, Brooks DJ, Hunot S, Joseph B, Deigendesch N, Garaschuk O, Boddeke E, Dinarello CA, Breitner JC, Cole GM, Golenbock DT, Kummer MP. Neuroinflammation in Alzheimer's disease. Lancet Neurol. 2015; 14:388–405. [PubMed: 25792098]
6. McCaulley ME, Grush KA. Alzheimer's disease: Exploring the role of inflammation and implications for treatment. Int J Alzheimers Dis. 2015; 2015:515248. [PubMed: 26664821]
7. Varma VR, Varma S, An Y, Hohman TJ, Seddighi S, Casanova R, Beri A, Dammer EB, Seyfried NT, Pletnikova O, Moghekar A, Wilson MR, Lah JJ, O'Brien RJ, Levey AI, Troncoso JC, Albert MS, Thambisetty M. Alpha-2 macroglobulin in Alzheimer's disease: A marker of neuronal injury through the RCAN1 pathway. Mol Psychiatry. 2017; 22:13–23. [PubMed: 27872486]
8. Kucukdereli H, Allen NJ, Lee AT, Feng A, Ozlu MI, Conatser LM, Chakraborty C, Workman G, Weaver M, Sage EH, Barres BA, Eroglu C. Control of excitatory CNS synaptogenesis by astrocyte-secreted proteins Hevin and SPARC. Proc Natl Acad Sci U S A. 2011; 108:E440–E449. [PubMed: 21788491]
9. Eroglu C. The role of astrocyte-secreted matricellular proteins in central nervous system development and function. J Cell Commun Signal. 2009; 3:167–176. [PubMed: 19904629]
10. Jones EV, Bouvier DS. Astrocyte-secreted matricellular proteins in CNS remodelling during development and disease. Neural Plast. 2014; 2014:321209. [PubMed: 24551460]
11. McKinnon PJ, Margolskee RF. SC1: A marker for astrocytes in the adult rodent brain is upregulated during reactive astrocytosis. Brain Res. 1996; 709:27–36. [PubMed: 8869553]
12. Purcell AE, Jeon OH, Zimmerman AW, Blue ME, Pevsner J. Postmortem brain abnormalities of the glutamate neurotransmitter system in autism. Neurology. 2001; 57:1618–1628. [PubMed: 11706102]
13. Hammack BN, Fung KY, Hunsucker SW, Duncan MW, Burgoon MP, Owens GP, Gilden DH. Proteomic analysis of multiple sclerosis cerebrospinal fluid. Mult Scler. 2004; 10:245–260. [PubMed: 15222687]
14. Jacquemont ML, Sanlaville D, Redon R, Raoul O, Cormier-Daire V, Lyonnet S, Amiel J, Le Merrer M, Heron D, de Blois MC, Prieur M, Vekemans M, Carter NP, Munnich A, Colleaux L, Philippe A. Array-based comparative genomic hybridisation identifies high frequency of cryptic chromosomal rearrangements in patients with syndromic autism spectrum disorders. J Med Genet. 2006; 43:843–849. [PubMed: 16840569]

15. Kähler AK, Djurovic S, Kulle B, Jönsson EG, Agartz I, Hall H, Opjordsmoen S, Jakobsen KD, Hansen T, Melle I, Werge T, Steen VM, Andreassen OA. Association analysis of schizophrenia on 18 genes involved in neuronal migration: MDGA1 as a new susceptibility gene. Am J Med Genet B Neuropsychiatr Genet. 2008; 147B:1089–1100. [PubMed: 18384059]
16. Vialou V, Robison AJ, Laplant QC, Covington HE 3rd, Dietz DM, Ohnishi YN, Mouzon E, Rush AJ 3rd, Watts EL, Wallace DL, Iniguez SD, Ohnishi YH, Steiner MA, Warren BL, Krishnan V, Bolaños CA, Neve RL, Ghose S, Berton O, Tamminga CA, Nestler EJ. DeltaFosB in brain reward circuits mediates resilience to stress and antidepressant responses. Nat Neurosci. 2010; 13:745–752. [PubMed: 20473292]
17. Zhurov V, Stead JD, Merali Z, Palkovits M, Faludi G, Schild-Poulter C, Anisman H, Poulter MO. Molecular pathway reconstruction and analysis of disturbed gene expression in depressed individuals who died by suicide. PLoS One. 2012; 7:e47581. [PubMed: 23110080]
18. Risher WC, Patel S, Kim IH, Uezu A, Bhagat S, Wilton DK, Pilaz LJ, Singh Alvarado J, Calhan OY, Silver DL, Stevens B, Calakos N, Soderling SH, Eroglu C. Astrocytes refine cortical connectivity at dendritic spines. Elife. 2014; 3doi: 10.7554/eLife.04047
19. Yin GN, Lee HW, Cho JY, Suk K. Neuronal pentraxin receptor in cerebrospinal fluid as a potential biomarker for neurodegenerative diseases. Brain Res. 2009; 1265:158–170. [PubMed: 19368810]
20. Vafadar-Isfahani B, Ball G, Coveney C, Lemetre C, Boocock D, Minthon L, Hansson O, Miles AK, Janciauskiene SM, Warden D, Smith AD, Wilcock G, Kalsheker N, Rees R, Matharoo-Ball B, Morgan K. Identification of SPARC-like 1 protein as part of a biomarker panel for Alzheimer's disease in cerebrospinal fluid. J Alzheimers Dis. 2012; 28:625–636. [PubMed: 22045497]
21. Richens JL, Vere KA, Light RA, Soria D, Garibaldi J, Smith AD, Warden D, Wilcock G, Bajaj N, Morgan K, O'Shea P. Practical detection of a definitive biomarker panel for Alzheimer's disease; comparisons between matched plasma and cerebrospinal fluid. Int J Mol Epidemiol Genet. 2014; 5:53–70. [PubMed: 24959311]
22. Shankar GM, Walsh DM. Alzheimer's disease: Synaptic dysfunction and Abeta. Mol Neurodegener. 2009; 4:48. [PubMed: 19930651]
23. Clarke LE, Barres BA. Emerging roles of astrocytes in neural circuit development. Nat Rev Neurosci. 2013; 14:311–321. [PubMed: 23595014]
24. ExplainBio, http://www.explainbio.com/, Accessed Accessed 15 September 2016.
25. Varma, S. Network model of normal gene expression predicts gene perturbation fold changes. 8th Annual RECOMB/ISCB Conference on Regulatory and Systems Genomics with DREAM Challenges 2015; Philadelphia, PA. 2015. p. 78-79.
26. Gene-Tissue Expression Project (GTEx) Portal. http://www.gtexportal.org/home/, Accessed 1 September 2016
27. Storey JD, Tibshirani R. Statistical significance for genomewide studies. Proc Natl Acad Sci U S A. 2003; 100:9440–9445. [PubMed: 12883005]
28. Broad Institute SNP Annotation and Proxy Search. http://archive.broadinstitute.org/mpg/snap/ldsearchpw.php, Accessed 1 October 2017
29. Terracciano A, Balaci L, Thayer J, Scally M, Kokinos S, Ferrucci L, Tanaka T, Zonderman AB, Sanna S, Olla N, Zuncheddu MA, Naitza S, Busonero F, Uda M, Schlessinger D, Abecasis GR, Costa PT Jr. Variants of the serotonin transporter gene and NEO-PI-R Neuroticism: No association in the BLSA and SardiNIA samples. Am J Med Genet B Neuropsychiatr Genet. 2009; 150B:1070–1077. [PubMed: 19199283]
30. Stone JL, Norris AH. Activities and attitudes of participants in the Baltimore longitudinal study. J Gerontol. 1966; 21:575–580. [PubMed: 5918312]
31. Fabbri E, An Y, Zoli M, Tanaka T, Simonsick EM, Kitner-Triolo MH, Studenski SA, Resnick SM, Ferrucci L. Association between accelerated multimorbidity and age-related cognitive decline in older Baltimore Longitudinal Study of Aging participants without dementia. J Am Geriatr Soc. 2016; 64:965–972. [PubMed: 27131225]
32. Petersen RC. Mild cognitive impairment as a diagnostic entity. J Intern Med. 2004; 256:183–194. [PubMed: 15324362]
33. Williams, J. American Psychiatric Association. Washington, DC: 1987.

34. McKhann G, Drachman D, Folstein M, Katzman R, Price D, Stadlan EM. Clinical diagnosis of Alzheimer's disease: Report of the NINCDS-ADRDA Work Group under the auspices of Department of Health and Human Services Task Force on Alzheimer's Disease. Neurology. 1984; 34:939–944. [PubMed: 6610841]
35. Blessed G, Tomlinson BE, Roth M. The association between quantitative measures of dementia and of senile change in the cerebral grey matter of elderly subjects. Br J Psychiatry. 1968; 114:797–811. [PubMed: 5662937]
36. Morris JC. Clinical dementia rating: A reliable and valid diagnostic and staging measure for dementia of the Alzheimer type. Int Psychogeriatr. 1997; 9(Suppl 1):173–176. discussion 177-178. [PubMed: 9447441]
37. Radloff LS. The use of the Center for Epidemiologic Studies Depression Scale in adolescents and young adults. J Youth Adolesc. 1991; 20:149–166. [PubMed: 24265004]
38. Ferrucci L. The Baltimore Longitudinal Study of Aging (BLSA): A 50-year-long journey and plans for the future. J Gerontol A Biol Sci Med Sci. 2008; 63:1416–1419. [PubMed: 19126858]
39. Shock, NW., Gerontology Research Center (U.S.). Normal human aging: The Baltimore Longitudinal Study of Aging. U.S. Dept. of Health and Human Services, Public Health Service, National Institutes of Health, National Institute on Aging For sale by the Supt of Docs., U.S G.P.O.; Baltimore, Md, Washington, D.C: 1984.
40. Resnick SM, Goldszal AF, Davatzikos C, Golski S, Kraut MA, Metter EJ, Bryan RN, Zonderman AB. One-year age changes in MRI brain volumes in older adults. Cereb Cortex. 2000; 10:464–472. [PubMed: 10847596]
41. Resnick SM, Pham DL, Kraut MA, Zonderman AB, Davatzikos C. Longitudinal magnetic resonance imaging studies of older adults: A shrinking brain. J Neurosci. 2003; 23:3295–3301. [PubMed: 12716936]
42. Goldszal AF, Davatzikos C, Pham DL, Yan MX, Bryan RN, Resnick SM. An image-processing system for qualitative and quantitative volumetric analysis of brain images. J Comput Assist Tomogr. 1998; 22:827–837. [PubMed: 9754125]
43. Shen D, Davatzikos C. HAMMER: Hierarchical attribute matching mechanism for elastic registration. IEEE Trans Med Imaging. 2002; 21:1421–1439. [PubMed: 12575879]
44. Driscoll I, Davatzikos C, An Y, Wu X, Shen D, Kraut M, Resnick SM. Longitudinal pattern of regional brain volume change differentiates normal aging from MCI. Neurology. 2009; 72:1906–1913. [PubMed: 19487648]
45. Pengas G, Pereira JM, Williams GB, Nestor PJ. Comparative reliability of total intracranial volume estimation methods and the influence of atrophy in a longitudinal semantic dementia cohort. J Neuroimaging. 2009; 19:37–46. [PubMed: 18494772]
46. Beason-Held LL, Kraut MA, Resnick SM. I. Longitudinal changes in aging brain function. Neurobiol Aging. 2008; 29:483–496. [PubMed: 17184881]
47. Hartley HO, Rao JN. Maximum-likelihood estimation for the mixed analysis of variance model. Biometrika. 1967; 54:93–108. [PubMed: 6049561]
48. Simpson BN, Kim M, Chuang YF, Beason-Held L, Kitner-Triolo M, Kraut M, Lirette ST, Windham BG, Griswold ME, Legido-Quigley C, Thambisetty M. Blood metabolite markers of cognitive performance and brain function in aging. J Cereb Blood Flow Metab. 2016; 36:1212–1223. [PubMed: 26661209]
49. Mendis DB, Ivy GO, Brown IR. SC1, a brain extracellular matrix glycoprotein related to SPARC and follistatin, is expressed by rat cerebellar astrocytes following injury and during development. Brain Res. 1996; 730:95–106. [PubMed: 8883893]
50. Weimer JM, Stanco A, Cheng JG, Vargo AC, Voora S, Anton ES. A BAC transgenic mouse model to analyze the function of astroglial SPARCL1 (SC1) in the central nervous system. Glia. 2008; 56:935–941. [PubMed: 18381651]
51. Xu PT, Li YJ, Qin XJ, Scherzer CR, Xu H, Schmechel DE, Hulette CM, Ervin J, Gullans SR, Haines J, Pericak-Vance MA, Gilbert JR. Differences in apolipoprotein E3/3 and E4/4 allele-specific gene expression in hippocampus in Alzheimer disease. Neurobiol Dis. 2006; 21:256–275. [PubMed: 16198584]

52. Klingberg T, Kawashima R, Roland PE. Activation of multi-modal cortical areas underlies short-term memory. Eur J Neurosci. 1996; 8:1965–1971. [PubMed: 8921287]
53. Klingberg T. Concurrent performance of two working memory tasks: Potential mechanisms of interference. Cereb Cortex. 1998; 8:593–601. [PubMed: 9823480]
54. Salo E, Rinne T, Salonen O, Alho K. Brain activity during auditory and visual phonological, spatial and simple discrimination tasks. Brain Res. 2013; 1496:55–69. [PubMed: 23261663]
55. Grady CL, McIntosh AR, Rajah MN, Beig S, Craik FI. The effects of age on the neural correlates of episodic encoding. Cereb Cortex. 1999; 9:805–814. [PubMed: 10600999]
56. Madden DJ, Gottlob LR, Allen PA. Adult age differences in visual search accuracy: Attentional guidance and target detectability. Psychol Aging. 1999; 14:683–694. [PubMed: 10632154]
57. Beason-Held LL, Goh JO, An Y, Kraut MA, O'Brien RJ, Ferrucci L, Resnick SM. Changes in brain function occur years before the onset of cognitive impairment. J Neurosci. 2013; 33:18008–18014. [PubMed: 24227712]
58. Sepulcre J, Sabuncu MR, Becker A, Sperling R, Johnson KA. In vivo characterization of the early states of the amyloid-beta network. Brain. 2013; 136:2239–2252. [PubMed: 23801740]
59. Johnson KA, Schultz A, Betensky RA, Becker JA, Sepulcre J, Rentz D, Mormino E, Chhatwal J, Amariglio R, Papp K, Marshall G, Albers M, Mauro S, Pepin L, Alverio J, Judge K, Philiossaint M, Shoup T, Yokell D, Dickerson B, Gomez-Isla T, Hyman B, Vasdev N, Sperling R. Tau positron emission tomographic imaging in aging and early Alzheimer disease. Ann Neurol. 2016; 79:110–119. [PubMed: 26505746]
60. Sojkova J, Beason-Held L, Zhou Y, An Y, Kraut MA, Ye W, Ferrucci L, Mathis CA, Klunk WE, Wong DF, Resnick SM. Longitudinal cerebral blood flow and amyloid deposition: An emerging pattern? J Nucl Med. 2008; 49:1465–1471. [PubMed: 18703614]
61. Sperling RA, Laviolette PS, O'Keefe K, O'Brien J, Rentz DM, Pihlajamaki M, Marshall G, Hyman BT, Selkoe DJ, Hedden T, Buckner RL, Becker JA, Johnson KA. Amyloid deposition is associated with impaired default network function in older persons without dementia. Neuron. 2009; 63:178–188. [PubMed: 19640477]
62. Bero AW, Yan P, Roh JH, Cirrito JR, Stewart FR, Raichle ME, Lee JM, Holtzman DM. Neuronal activity regulates the regional vulnerability to amyloid-deposition. Nat Neurosci. 2011; 14:750–756. [PubMed: 21532579]
63. Bakker A, Krauss GL, Albert MS, Speck CL, Jones LR, Stark CE, Yassa MA, Bassett SS, Shelton AL, Gallagher M. Reduction of hippocampal hyperactivity improves cognition in amnestic mild cognitive impairment. Neuron. 2012; 74:467–474. [PubMed: 22578498]
64. Tackenberg C, Grinschgl S, Trutzel A, Santuccione AC, Frey MC, Konietzko U, Grimm J, Brandt R, Nitsch RM. NMDA receptor subunit composition determines beta-amyloid-induced neurodegeneration and synaptic loss. Cell Death Dis. 2013; 4:e608. [PubMed: 23618906]
65. Rudy CC, Hunsberger HC, Weitzner DS, Reed MN. The role of the tripartite glutamatergic synapse in the pathophysiology of Alzheimer's disease. Aging Dis. 2015; 6:131–148. [PubMed: 25821641]
66. Craig AM, Kang Y. Neurexin-neuroligin signaling in synapse development. Curr Opin Neurobiol. 2007; 17:43–52. [PubMed: 17275284]
67. Singh SK, Stogsdill JA, Pulimood NS, Dingsdale H, Kim YH, Pilaz LJ, Kim IH, Manhaes AC, Rodrigues WS Jr, Pamukcu A, Enustun E, Ertuz Z, Scheiffele P, Soderling SH, Silver DL, Ji RR, Medina AE, Eroglu C. Astrocytes assemble thalamocortical synapses by bridging NRX1 and NL1 via hevin. Cell. 2016; 164:183–196. [PubMed: 26771491]

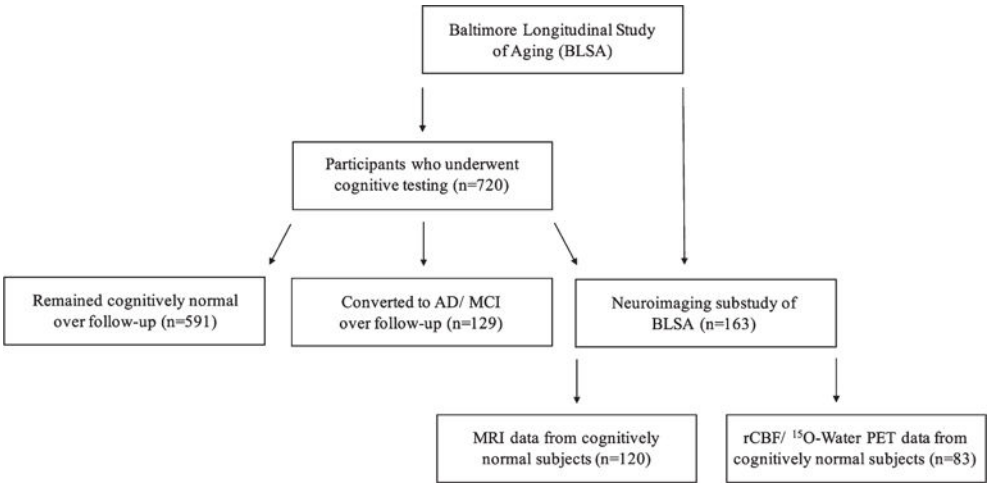

Fig. 1.

Overview of study design. Flow chart summarizing the selection of participants from the BLSA whose longitudinal neuroimaging and cognitive performance data were analyzed in this study. The major aims of this study were to examine associations between SNPs in the *SPARCL1* gene and longitudinal changes in 1) cognitive performance, 2) MRI-derived brain volumes, and 3) ^{15}O-water PET-derived resting-state cerebral blood flow.

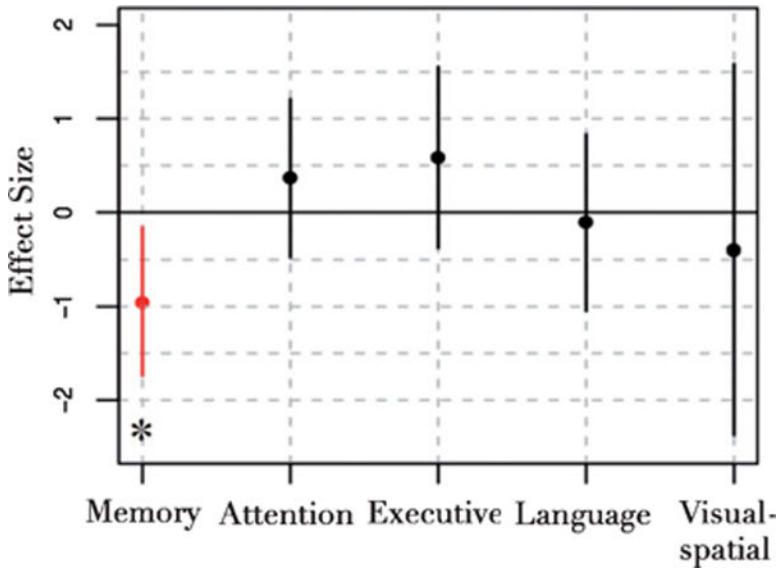

Fig. 2.

Associations between rs7695558 SNP in the *SPARCL1* gene and longitudinal changes in cognitive performance in converters to MCI/AD. Dot plots of effect sizes and corresponding 95% confidence intervals showing associations between *SPARCL1* SNP rs7695558 and rates of change in domain-specific cognitive performance. Individuals in the converter group who carried the minor allele of the *SPARCL1* rs7695558 variant showed significantly faster rates of decline in memory performance (red dot) relative to non-carriers.

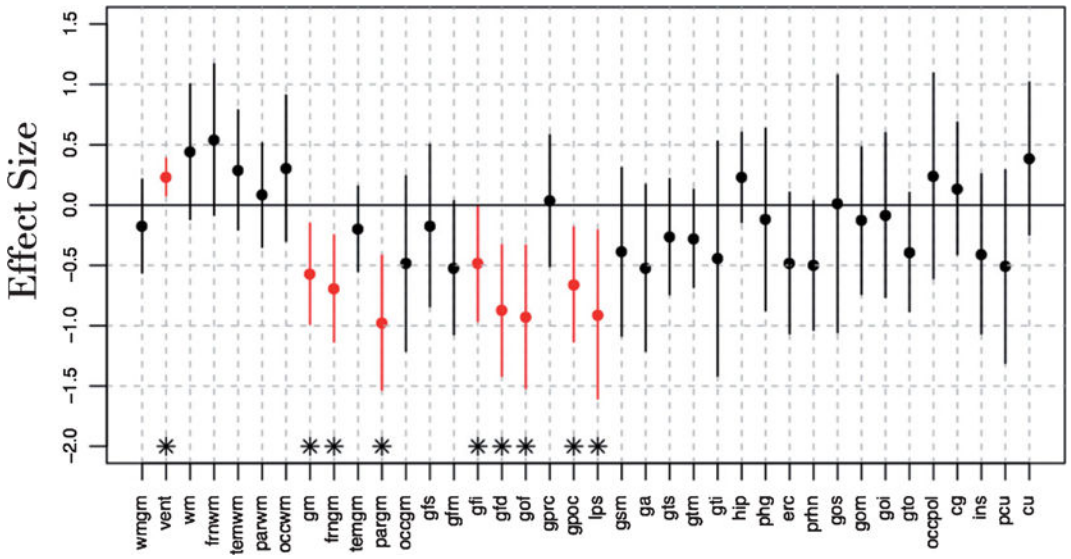

Fig. 3.

Associations between longitudinal changes in brain volumes and rs9998212 SNP in the *SPARCL1* gene in cognitively normal older individuals. Dot plots of effect sizes and corresponding 95% confidence intervals (CI) showing associations between *SPARCL1* SNP rs9998212 and rates of change in brain volumes. Statistically significant effects (red dots) are seen in regions where the 95% CI does not cross the zero reference line. WMGM, whole brain; VENT, whole ventricular volume; WM, white matter; FRNWM, frontal white matter; TEMWM, temporal white matter; PARWM, parietal white matter; OCCWM, occipital white matter; GM, gray matter; FRNGM, frontal gray matter; TEMGM, temporal gray matter; PARGM, parietal gray matter; OCCGM, occipital gray matter; GFS, superior frontal gyrus; GFM, middle frontal gyrus; GFI, inferior frontal gyrus; GFD, medial frontal gyrus; GOF, orbitofrontal gyrus; GPRC, pre-central sensorimotor cortex; GPOC, post-central sensorimotor cortex; LPS, superior parietal lobule; GSM, supramarginal gyrus; GA, angular gyrus; GTS, superior temporal gyrus; GTM, middle temporal gyrus; GTI, inferior temporal gyrus; HIP, hippocampus; PHG, parahippocampal gyrus; ERC, entorhinal cortex; PRHN, perirhinal cortex; GOS, superior occipital gyrus, GOM, middle occipital gyrus; GOI, inferior occipital gyrus; GTO, occipito-temporal gyrus; OCCPOL, occipital pole; CG, cingulate gyrus; INS, insula; PCU, precuneus; CU, cuneus.

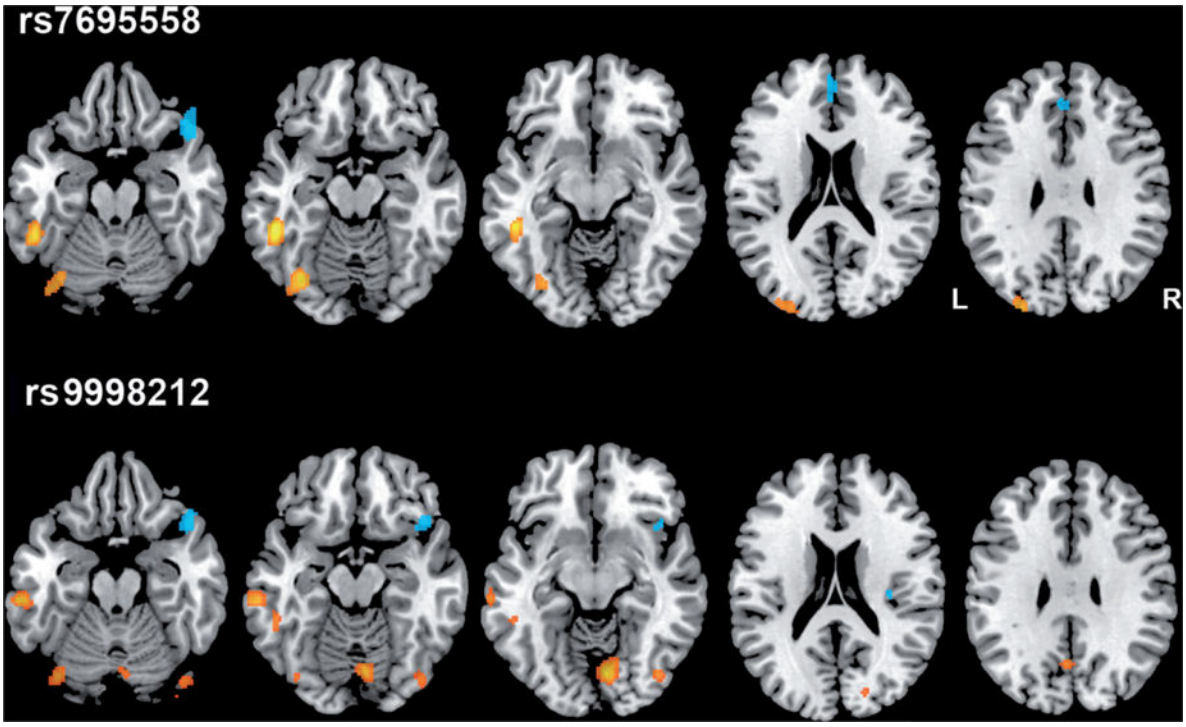

Fig. 4.

Longitudinal changes in regional resting-state cerebral blood flow (rCBF) associated with *SPARCL1* polymorphisms. Yellow and blue areas indicate significant longitudinal increases and decreases, respectively, in rCBF in minor allele carriers relative to non-carriers.

Table 1A

Sample characteristics of participants included in analysis of longitudinal cognitive performance. Fisher's Exact Test was used for comparing sex distributions. The Wilcoxon Rank-Sum Test was used for comparing all the other variables between the two groups

	No. subjects	No. data pts	No. visits	Follow-up interval (y)	Sex (female)	Baseline age (y)	Education (y)
Non-converters							
rs7695558 carriers	163	969	5.9 (3.8)	11.1 (6.8)	69 (42.3%)	62.6 (11.7)	16.4 (2.6)
rs7695558 non-carriers	428	2703	6.3 (3.9)	12.1 (6.9)	197 (46.0%)	60.8 (11.5)	16.4 (2.4)
p-value	N/A	N/A	0.312	0.089	0.460	0.085	0.867
rs9998212 carriers	169	968	5.7 (3.7)	10.7 (6.8)	71 (42.0%)	62.3 (11.4)	16.4 (2.4)
rs9998212 non-carriers	420	2692	6.4 (3.9)	12.3 (6.9)	194 (46.2%)	61.0 (11.7)	16.4 (2.4)
p-value	N/A	N/A	0.053	0.0090	0.362	0.110	0.829
Converters to MCI/AD							
rs7695558 carriers	32	190	5.9 (4.4)	8.8 (6.8)	14 (43.8%)	74.1 (6.4)	16.4 (2.8)
rs7695558 non-carriers	97	649	6.7 (4.4)	9.6 (6.2)	43 (44.3%)	72.6 (7.0)	16.4 (2.7)
p-value	N/A	N/A	0.347	0.468	1.00	0.305	0.960
rs9998212 carriers	37	255	6.9 (4.5)	10.0 (6.3)	17 (46.0%)	73.8 (6.5)	16.5 (2.4)
rs9998212 non-carriers	92	584	6.3 (4.4)	9.1 (6.4)	40 (43.5%)	72.7 (7.0)	16.4 (2.9)
p-value	N/A	N/A	0.456	0.411	0.846	0.441	0.844

Table 1B

Cognitive performance at baseline. T-tests were used for intergroup comparisons

	Memory	Attention	Executive function	Language	Visual-spatial	CESD
Non-converters						
rs7695558 carriers	0.16 (0.81)	0.06 (0.93)	0.04 (0.87)	0.04 (0.84)	0.04 (0.72)	5.44 (5.87)
rs7695558 non-carriers	0.18 (0.87)	0.04 (0.81)	0.09 (0.77)	0.07 (0.80)	0.15 (0.71)	5.80 (5.48)
p-value	0.797	0.787	0.571	0.635	0.115	0.494
rs9998212 carriers	0.14 (0.84)	0.03 (0.93)	0.10 (0.85)	0.07 (0.83)	0.06 (0.75)	5.59 (5.81)
rs9998212 non-carriers	0.19 (0.87)	0.05 (0.81)	0.07 (0.78)	0.06 (0.80)	0.14 (0.71)	5.73 (5.51)
p-value	0.519	0.813	0.679	0.972	0.223	0.784
Converters to MCI/AD						
rs7695558 carriers	−0.34 (0.98)	−0.47 (0.98)	−0.40 (0.79)	−0.03 (0.83)	−0.43 (0.79)	5.43 (6.27)
rs7695558 non-carriers	−0.42 (0.97)	−0.54 (0.82)	−0.54 (0.98)	−0.19 (0.77)	−0.25 (0.66)	6.35 (7.18)
p-value	0.727	0.698	0.468	0.309	0.259	0.534
rs9998212 carriers	−0.28 (0.89)	−0.62 (0.96)	−0.48 (0.80)	−0.05 (0.75)	−0.32 (0.74)	5.40 (5.95)
rs9998212 non-carriers	−0.46 (0.99)	−0.48 (0.82)	−0.51 (0.99)	−0.20 (0.80)	−0.27 (0.67)	6.42 (7.34)
p-value	0.390	0.387	0.888	0.323	0.734	0.468

Table 2

Sample characteristics of participants included in the MRI and ^{15}O-water PET studies. Fisher's Exact Test was used to compare sex distributions. Wilcoxon rank-sum test was used to compare all the other variables between the two groups

	No. subjects	No. data pts	No. visits	Follow-up interval (y)	Sex (female)	Baseline age (y)	Education (y)
MRI							
rs7695558 carriers	30	212	7.1 (2.0)	6.9 (2.2)	10 (33.3%)	71.9 (7.9)	15.7 (3.5)
rs7695558 non-carriers	90	614	6.8 (2.8)	6.3 (2.9)	36 (40.0%)	69.9 (8.2)	16.6 (2.5)
p-value	N/A	N/A	0.595	0.793	0.665	0.295	0.255
rs9998212 carriers	35	248	7.1 (2.1)	6.8 (2.2)	11 (31.4%)	71.8 (7.6)	16.2 (2.9)
rs9998212 non-carriers	85	578	6.8 (2.9)	6.3 (2.9)	35 (41.2%)	69.9 (8.3)	16.5 (2.8)
p-value	N/A	N/A	0.708	0.947	0.410	0.199	0.584
^{15}O-Water PET							
rs7695558 carriers	21	165	7.9 (1.3)	7.7 (1.4)	8 (38.1%)	70.8 (8.2)	15.6 (3.8)
rs7695558 non-carriers	60	499	8.3 (0.9)	7.8 (0.8)	24 (40.0%)	69.0 (7.2)	16.5 (2.4)
p-value	N/A	N/A	0.212	0.573	1.00	0.566	0.565
rs9998212 carriers	24	189	7.9 (1.4)	7.5 (1.4)	9 (37.5%)	71.6 (7.6)	16.2 (3.2)
rs9998212 non-carriers	57	475	8.3 (0.8)	7.8 (0.8)	23 (40.4%)	68.6 (7.3)	16.3 (2.7)
p-value	N/A	N/A	0.389	0.456	1.00	0.119	0.987

Table 3

Longitudinal changes in regional resting-state cerebral blood flow (rCBF) associated with *SPARCL1* polymorphisms. Local maxima within areas of significant longitudinal decreases and increases in rCBF in carriers of the minor allele of the rs7695558 and rs9998212 variants. Coordinates are in stereotactic space and Brodmann areas are in parentheses

		Coordinates				
Region	**Side**	**X**	**Y**	**Z**	***p* value**	**Voxels**
rs7695558						
Decreased Activity						
Superior temporal gyrus (38)	R	46	24	−22	<0.001	150
Medial frontal cortex (9)	L	−2	38	26	<0.001	166
Orbitofrontal cortex (47)	L	−20	32	−24	<0.001	63
Increased Activity						
Inferior temporal gyrus (20)	L	−50	−50	−14	<0.001	275
Cerebellum	L	−34	−72	−16	<0.001	249
Cuneus (19)	L	−28	−90	26	<0.001	173
rs9998212						
Decreased Activity						
Anterior cingulate gyrus (32)	L	−16	44	0	<0.001	115
Superior temporal gyrus (38)	R	46	20	−20	<0.001	170
Insula	R	36	−14	14	0.001	55
Increased Activity						
Lingual gyrus (18)	R	10	−76	−2	<0.001	800
Inferior temporal gyrus (20)	L	−60	−28	−20	<0.001	263
Cerebellum	L	−38	−78	−20	0.001	120
Precuneus (7)	L	−2	−64	34	0.001	69
Middle occipital gyrus (19)	R	40	−76	−6	0.001	218